Vanessa Velasco
Andrew H. Work Jr.
Stuart J. Williams

University of Louisville, Department of Mechanical Engineering, Louisville, Kentucky, USA

Received December 9, 2011
Revised February 1, 2012
Accepted February 3, 2012

Research Article

Electrokinetic concentration and patterning of colloids with a scanning laser

Optically-based lab-on-a-chip systems have the distinct advantage of being dynamically controlled in real time, providing reconfigurable operations that can be tuned to perform a variety of tasks. This manuscript demonstrates the concentration of liquid-suspended microparticles using a focused near-infrared laser (980 nm) and a parallel-plate electrode system. The parallel-plate electrodes consisted of an indium tin oxide-coated coverslip and a gold-coated glass substrate. When the laser was applied at 36 mW, the indium tin oxide surface is locally heated creating sharp temperature gradients on the order of $0.07^{\circ}C/\mu m$. When an AC field was applied, electrothermal hydrodynamic forces generated microfluidic vortices. At an AC frequency of 40 kHz, the optically controlled electro-hydrodynamics aggregated colloids at the center of fluid motion on the surface of the indium tin oxide coverslip. The nature of colloid aggregation, translation, and patterning was explored when the translational velocity of the laser spot was varied. This manuscript describes the design of the laser scanning system using commercially available components and the fabrication of the parallel-plate chip. The effect that the laser scanning rate has on the heat transfer, fluid velocity, and colloid aggregation is discussed.

Keywords:
Colloids / Electrohydrodynamics / Electrothermal / Microfluidics / Patterning
DOI 10.1002/elps.201100676

1 Introduction

Electrokinetic concentration and control of liquid-suspended micro- and nanoparticles provide dynamic non-contact methods of colloid manipulation for lab-on-a-chip devices. In particular, AC electrokinetic techniques are advantageous due to their frequency-dependent physical mechanisms, enabling an additional degree of freedom to tune the electrokinetic physics for a particular sample. Dielectrophoresis is a well-studied electrokinetic mechanism that has significantly impacted microsystem technology development for various colloid manipulation schemes including the formation of artificial architectures [1, 2] and sorting of biological species [3]. AC electro-hydrodynamic mechanisms have also been used for microfluidic mixing [4] and pumping [5].

Electrokinetic mechanisms are typically integrated into devices with micrometer metal electrodes patterned through standard microfabrication techniques. Instead of permanent electrode features, recent advances have been made toward optically controlled electrokinetic techniques. Such methods enable the user to program and dynamically reconfigure the electrokinetic mechanisms. One such method is termed optoelectronic tweezers (OETs) in which a photoconductive material, typically hydrogenated amorphous silicon, coats one planar electrode within a parallel-plate configuration [6]. A micrometer-resolution illumination pattern is applied to this photoconductive layer, generating localized regions of increased electrical conductivity. To allow optical access, one or both electrodes are composed of indium tin oxide (ITO), a transparent conductive material. These "virtual" electrodes have generated dielectrophoretic forces to sort biological cells [7] or produce electro-hydrodynamic flows [8].

Rapid electrokinetic patterning (REP) is another optically controlled AC electrokinetic technique [9]. REP is similar to OET in that a parallel-plate configuration is used, but REP does not use photoconductive materials or other coatings on the electrode surface. As a result, the electric field across the sample remains uniform. A highly focused laser is applied to one electrode surface where it is absorbed, generating a localized hot spot. Temperature gradients within the medium

Correspondence: Dr. Stuart J. Williams, Assistant Professor, University of Louisville, Department of Mechanical Engineering, 200 Sackett Hall, Louisville, KY 40292, USA
E-mail: stuart.williams@louisville.edu
Fax: +1-502-852-6053

Abbreviations: **ITO**, indium tin oxide; **NIR**, near infrared; **OET**, optoelectronic tweezers; **REP**, rapid electrokinetic patterning; **μPIV**, micro particle image velocimetry

Colour Online: See the article online to view Figs. 1–4 in colour.

coupled with the applied AC field create electrothermal hydrodynamics and, in combination with particle–particle and particle–electrode electrokinetics, can concentrate, translate, pattern, and sort colloids [10]. A general discussion of REP electrokinetic mechanisms follows, but a more detailed explanation of its physics can be found elsewhere [10]. A recent review article on OET and REP applications and mechanisms is also available [11].

Previous REP work used a Nd:YAG laser-based optical trapping system (Bioryx® 200, Arryx Inc., Chicago, IL, USA), a specialized system that has the ability to generate and manipulate multiple traps using a computer-controlled spatial light modulator [12]. In REP, the generated light patterns heat the substrate only and do not optically trap particles; therefore, holographic or high-precision optical trapping components are not necessary, decreasing the overall cost of a dynamic REP system. Further, inexpensive optical trapping systems [13] could be minimally modified for REP applications.

This work expands upon previous REP investigations. This includes the design and assembly of a less expensive REP system that uses a scanning near-infrared (NIR) laser as its dynamic optical source. The electrothermal hydrodynamics and REP manipulation are characterized as a function of laser scanning speed, which affects the magnitude of optical absorption and transient heat transfer of the substrate. The temperature of the sample is measured using Rhodamine B, a temperature-dependent fluorescent dye. Next, electrothermal motion as a function of laser scanning speed is observed using micro particle image velocimetry (μPIV). Finally, the behavior of particle aggregation, translation, and patterning is explored. Previous work has explored electrothermal hydrodynamics and REP particle concentration as a function of AC frequency, AC voltage, and laser power [9, 10, 14, 15]; a general overview of REP physics follows.

REP investigations used a focused NIR laser (typically 1064 nm) to heat a targeted ITO electrode surface, although other wavelength/substrate combinations could be used to produce adequate localized heat generation. These nonuniform temperature regions would generate temperature gradients, which in turn would create gradients in the electrical properties of the fluid. When an AC field is applied in the presence of temperature gradients, electrothermal fluid motion would occur [16, 17]. Although Joule heating from the microelectrodes themselves is a typical method of inducing electrothermal hydrodynamics, external optically induced heating sources have also been demonstrated [18, 19]. For the case of REP, a hot spot located an electrode surface subjected to a uniform field will produce a three-dimensional, axisymmetric microfluidic vortex [15, 20]. Previous investigations demonstrated that effects of thermal convection on fluid flow due to optically induced heating were insignificant in the absence of an applied electric field. As a result, vortices were created only if the electric field was applied simultaneously with the laser spot. μPIV measurements showed that fluid velocity magnitude was proportional to the square of the applied voltage [15]. For this parallel-plate system, it was also observed that fluid velocity remained constant for AC frequencies below the medium's charge relaxation frequency, which is the ratio between its permittivity and conductivity [15, 20, 21].

The microfluidic vortex carried particles toward the electrode surface. At lower AC frequencies (typically less than 100 kHz), particle–electrode electrokinetic interactions produce an attractive force between them. Weak lateral forces allow the vortex to push the surface-trapped colloidal particles toward its center, where they aggregate. Therefore, the shape and characteristics of the electrothermal hydrodynamics are governed by the geometry and/or translation of trapped colloids. A balance of electrokinetic phenomena including dipole–dipole repulsive forces, particle-induced AC electroosmotic flow, dielectrophoresis, and ionic double layer polarization characterize the behavior of REP [10, 14, 22, 23] and is a subject of ongoing investigations.

2 Materials and methods

2.1 System

An illustration of the scanning laser REP system is shown in Fig. 1A. Optical components were integrated around the Nikon Eclipse Ti inverted microscope. A second epifluorescent turret feature was added to the microscope, this enabled one optical port for the fluorescence illumination and a second access for the NIR laser. The top filter cube was mounted with a hot mirror (z1064rdc, Chroma Technology Corp., Bellows Falls, VT, USA), a specialized dichroic mirror that allows visible light to pass and infrared wavelengths to be reflected. The lower filter cube received light emitted from an X-Cite 120 Fluorescence System and passed through an excitation filter cube allowing green light to be reflected off a dichroic mirror. The green illumination was delivered to the sample that excited red 1.0-μm fluorescent polystyrene microparticles (09–980-478, Thermo Scientific). The red fluorescence passed through the hot mirror and the dichroic and is received by a high performance 12-bit CCD camera (SensiCAM QE, PCO, Kelheim, Germany). All images and videos were acquired at frame rate of 18.72 Hz.

All components for the infrared scanning laser system were available through ThorLabs, Inc. (Newton, NJ, USA). A NIR laser diode operating at 980 nm (PL980P330 J) was mounted to a heat sink (LM14 S2) with electronic access for laser diode power (LDC210 C) and temperature (TEC200 C) control. The laser diode was coupled to an optical fiber that delivered the illumination to a port (PAF-X-7-B) converting the fiber output into a collimated beam. This port was mounted to a scanning mirror system (GVS002) consisting of two galvanometer-based scanning motors with an optical mirror mounted on each shaft. Up to a ±10 V input will rotate each mirror its full range of ±12.5°. A LabView (Austin, TX, USA) program was created that would send voltage signals to the mirrors to control their scanning velocity. For this investigation, the program swept the laser between two points separated approximately by 130 μm in an oscillatory manner with

periods varying from 25 ms to 66.7 s. Two lenses were used to expand the collimated laser beam from the scanning mirror before being delivered to the microscope. The optical system was aligned and attached to the back port of the microscope with a custom-machined bracket. The collimated laser was delivered to a 40× objective lens (0.6 NA). Assuming a Gaussian profile of the collimated laser, the minimum spot size through this objective is approximately 0.97 μm in diameter.

The laser power emitted from the fiber collimator (before the scanning mirrors) was measured and calibrated with respect to the settings on the laser diode controller. All stated optical powers within this manuscript are with respect to these measured values. The maximum power output of the laser diode was 330 mW; however, unless otherwise specified, the laser output was set to 36 mW. It was assumed that power loss through the galvanic mirrors, expanding optics, hot mirror, and objective lens was negligible.

The design for this scanning REP system was similar to that of an optical trapping system, as both use highly focused optics for operation. For REP, the goal was to create the sharpest illumination spot possible in order to generate large temperature gradients. However, unlike optical trapping, high numerical aperture lenses were not necessary to trap particles. On the contrary, in this study when high numerical aperture lenses were used, it was observed that optical trapping forces would repel particles from the electrode surface and prevent REP aggregation.

2.2 Chip fabrication

An illustration of REP within the parallel-plate microfluidic electrode chip is shown in Fig. 1B. The top electrode plate is composed of a chrome/gold layer (30 nm/180 nm) deposited on a microscope slide. The bottom plate consisted of an ITO-coated glass coverslip (170 μm thick) that was commercially available (SPI Supplies, West Chester, PA, USA). Two fluidic access holes were drilled into the gold-coated microscope slide. Between the microscope slide and cover slip was a 50-μm double-sided adhesive spacer that contained microfluidic features. Electrical leads were connected to each electrode and attached to a bench-top AC waveform generator (Model 3390, Keithley, Cleveland, OH, USA).

2.3 Temperature measurements

The resultant temperature profile from the optical heating was measured using Rhodamine B, a temperature-dependent fluorescent dye. Measuring temperature within a microfluidic device with a single dye has been demonstrated previously [24], including for monitoring Joule heating in an electrokinetic chip [25]. First, a calibration curve was obtained to determine the temperature-dependent fluorescent intensity behavior of the dye normalized with respect to room temperature. The room temperature Rhodamine B was injected into the parallel-plate device and ten sequential reference images were acquired without laser activation. Next, the laser was applied to the ITO surface and, after 1 min of activation, ten images were acquired. A MATLAB program averaged each set of reference and measurement images and compared the ratio of fluorescent intensities with the calibration curve to determine the temperature profile. However, at a laser power of 36 mW, detectible changes in fluorescent intensity were on the order of background noise. Thus, the optical power was increased to 212 mW for temperature measurements. Both static and transient measurements were taken.

For time-transient observations, sequential images were acquired at a rate of 18.72 frames per second. Room temperature dye was injected and the laser was deactivated at for the beginning of the image set. Next, the laser was activated and the step-input temperature response of the dye was recorded. This was repeated a second time except the laser was activated under a scanning program with a period of 15 Hz.

2.4 Sample preparation

A particle solution was made by mixing 80 μL of 1.0-μm red fluorescent polystyrene particles (1% particle solids) in 4.0 mL of an aqueous solution of potassium chloride (KCl)

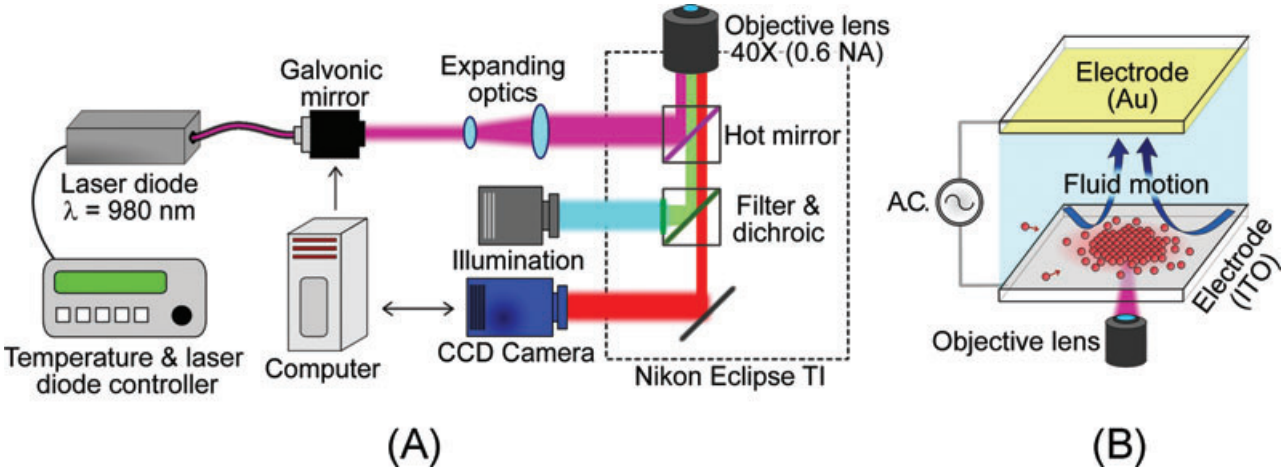

Figure 1. (A) Illustration of the scanning mirror REP system. (B) Illustration of particles captured with REP within a parallel-plate chip.

containing 0.05% Tween 20 with a measured conductivity of 2.5 mS/m. Approximately an hour prior to beginning the experiments, the channel was flushed and primed with a similar KCl solution containing no particles. The same particle suspension was used for both REP and fluid velocimetry studies. A fresh sample of particles was introduced between experiments.

2.5 Particle image velocimetry

The velocity of the electrothermal microfluidic vortex was measured using μPIV. This procedure is similar to a previous observation from electrothermal vortices generated from a spatial light modulator system [15]. As previously mentioned, REP particle aggregation shape and translation mechanics are governed by hydrodynamic lateral forces. Therefore, fluid velocimetry measurements were acquired at the plane of particle aggregation, which is just above the ITO surface. A sample containing tracer particles was manually injected. Then, an AC signal of 500 kHz and 3.6 V_{rms} was applied. The AC frequency was greater than that of REP to minimize the effects of particle–electrode attractive forces. The electrothermal fluid velocity at 500 kHz and lower frequencies will remain constant, as this frequency range is below the medium's charge relaxation frequency [15]. The applied laser power was 36 mW and the scanning rate ranged from 25 ms oscillation periods to static conditions. Approximately 334 images were acquired sequentially at 18.72 frames per second for each trial. Recorded images were processed using a PIV software program developed by Linchuan Gui [26].

2.6 Colloid trapping and manipulation

REP is a frequency-dependent method. Aggregation usually takes place at frequencies below 100 kHz due to dominating attractive particle–electrode forces. However, particle aggregations become unstable and trapped particles are released as the AC frequency is increased above its trapping frequency. Here, fluid drag overcomes electrokinetic attractive forces, causing the particles to be carried away by the toroidal vortex [10]. For this study, colloidal concentration, translation, and patterning occurred at an AC signal of 40 kHz and 3.6 V_{rms} with an optical power of 36 mW. Images were extracted from videos acquired at a rate of 18.72 frames per second. The laser scanning period ranged from 25 ms to 66.7 s.

3 Results and discussion

3.1 Temperature measurements

The measured temperature profile just above the ITO surface for an applied laser power of 212 mW is shown in Fig. 2A. Each data point represents a measured pixel temperature value of a line crossing through the peak of the profile; the line was fit with respect to a Lorenz peak. Both μPIV and REP experiments were conducted at a reduced optical power. It was assumed that the magnitude of the temperature profile was directly proportional to optical heating power, meaning that the temperature profile for the 36 mW applied laser would be approximately 17% of the measured value at 212 mW. This would correspond with a peak value of 6.1°C and a maximum temperature gradient of 0.07°C/μm.

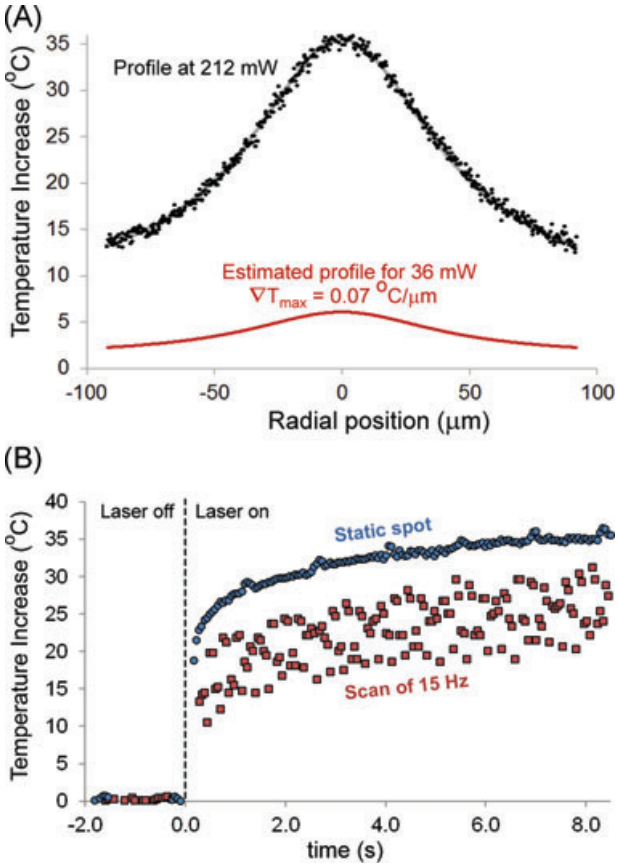

Figure 2. (A) Measured temperature profile taken from the cross section that intersects the center of a static laser spot at a power of 212 mW. An estimated temperature profile is provided for an illumination of 36 mW. (B) Time-transient peak temperature of a static and scanned laser at 212 mW.

Figure 2B shows the time-transient temperature response when a 212 mW laser is applied for a static and a 15-Hz scanning case. The peak temperature of the static case resembles a step-input response, as expected. The peak temperature of the scanning case was monitored at the midpoint between laser oscillation endpoints during scanning operation. Here, the temperature oscillates between a maximum and minimum value while exhibiting similar characteristics to the step-input case. For larger scanning periods, the range of temperature value extends, with the maximum value being bound by the step-input response (data not shown). It is hypothesized that as the scanning rate increases, the range of temperatures would converge; this will occur for

laser scanning periods approaching the rate of device heat dissipation.

The temperature profile itself is important for analysis and design of electrothermal hydrodynamic systems. Further, the oscillatory nature of the temperature field for a scanning laser presents two results. The first, and obvious, observation is that the overall temperature is less than that of a static spot. This will produce weaker electrothermal fluid velocities leading to less compact REP aggregations. Optical power could be increased to overcome this limitation. Second, the oscillatory nature of the temperature field will generate localized oscillations in the electrothermal velocity field during rapid periodic scans. This is intriguing from a fluid dynamics perspective and investigators could potentially use this characteristic for enhanced mixing or sorting of particles based on hydrodynamic drag.

It is important to note the limitation of the Rhodamine B measurement technique for this experiment. The measured temperature profile, and thus temperature gradients, was an underestimation of the actual temperature gradients. This is due to the fact that the measurement region is a depth-averaged measurement of the fluorescent dye imaged within the depth of the viewing plane. Therefore the out-of-plane temperature variations were not accounted for, reducing the overall measured values.

3.2 Particle image velocimetry

Figure 3 shows the time-averaged measured fluid velocimetry profiles just above the ITO electrode for (A) a static laser spot and (B) one that is scanned with a period of 25 ms. Each measurement occurred for a laser power of 36 mW and an AC signal of 500 kHz and 3.6 V_{rms}. A static laser produced an axisymmetric vortex whereas the velocimetry profile of the scanned laser produced an elliptical vortex with weaker fluid velocimetry. Hence, the fluid velocity patterns can be generated with computer-controlled laser scanning geometries.

What is not discernible from Fig. 3B was the fluid velocity at a particular point was not constant with a scanned laser, as the temperature itself is not constant (Fig. 2B). The maximum velocity of the fluid as well as the range of fluid velocities varies as a function of the scanning period. Figure 3C shows the maximum electrothermal velocity as a function of scanned laser period. To investigate the variability in fluid velocity, the velocity of an arbitrary point 20 μm from the vortex center was extracted from each image pair from the 334 sequential image set. Its median absolute deviation for the image set was calculated for each scan speed (Fig. 3C). The slower scanning speeds produced larger overall heating which, in turn, generated larger temperature gradients and greater electrothermal fluid velocities. The slower scanning rates, in turn, also allowed previously scanned regions to decrease in temperature further, lowering the localized velocity producing greater overall flow variability during the scan period. The range of fluid velocities converged to a lower value as scan rate increased.

Videos demonstrating electrothermal hydrodynamic behavior for a laser scan at periods of 25 ms, 67 ms, 1.0 s, 6.7 s, and 66.7 s are available in Supporting Information.

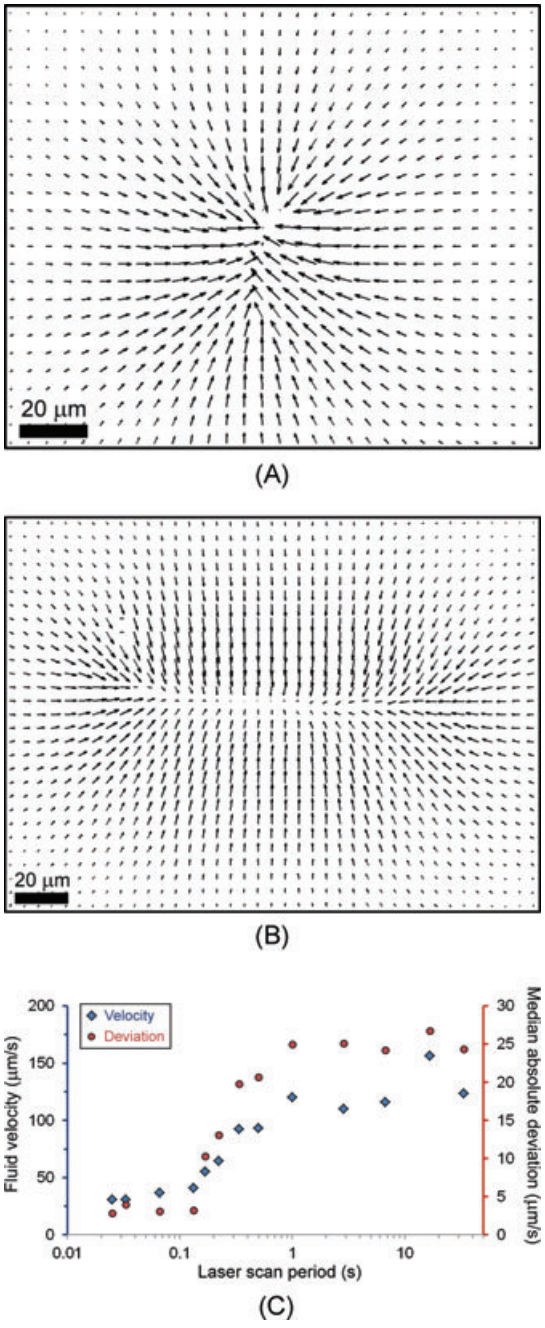

Figure 3. Micro PIV for (A) a static spot and (B) a scanning line with a period of 25 ms. The velocity profile was averaged over a period of 17.8 s, corresponding to the sequentially acquired 334 images. (C) The maximum measured fluid velocity and its deviation for various scanning periods. Images were acquired with an optical power of 36 mW an AC signal of 500 Hz and 3.6 V_{rms} at 18.72 frames per second.

3.3 Colloid trapping and manipulation

Particle aggregation, translation, and patterning for REP is governed by electrothermal hydrodynamics. Previous patterning investigations had a steady illumination geometry [9] whereas this work investigated the use of a scanning laser. The unsteady nature of electrothermal hydrodynamics using a scanning laser influenced particle aggregation behavior. The same sample of 1.0-μm particles underwent REP when the AC frequency was decreased to 40 kHz. The colloid aggregation behavior can be generalized in four categories, as illustrated in Fig. 4. First is a static spot (Fig. 4A) that is characterized with high fluid velocities resulting in more compact particle aggregations as the larger fluid drag overcomes weaker dipole–dipole repulsive forces. Electrokinetic characterization of a static spot has been investigated previously [10, 14]. The second case is when the velocity of the laser scan is less than the electrothermal fluid velocity (Fig. 4B). Here, the aggregation has adequate time to follow the path of the laser resulting in translation of the colloid group.

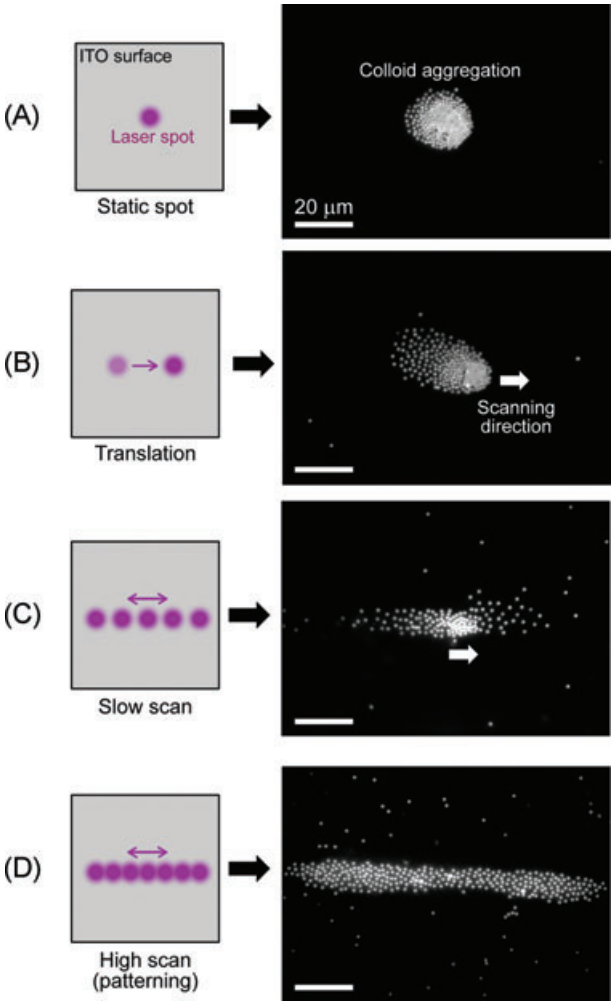

Figure 4. REP behavior for (A) a static or (B–D) scanned laser spot with decreasing scanning periods. The left panel indicates the location and/or translation of the laser spot. The arrows indicate the direction of laser motion.

The behavior of REP becomes more complex once the speed of the scanning laser is on the order of or faster than the electrothermal fluid velocity. At moderate scan rates, the colloids were carried to the trapping region and were briefly trapped and translated with the scanning laser; however, due to dipole–dipole repulsive forces and decreased hydrodynamic drag attractive forces, these particles were quickly released (Fig. 4C). As the laser scan period decreased, the temperature profile became steadier, resulting in more stable electrothermal flows and consequently a steady colloidal aggregation pattern. However, even at a scanning period of 25 ms, there were fluctuations in temperature that led to rapid and brief localized pulsations and instability within the particle aggregation. Future investigations will explore this phenomenon with the use of a high-speed camera.

Videos demonstrating REP behavior for laser scan periods of 25 ms, 67 ms, 1.0 s, 6.7 s, and 66.7 s are available in Supporting Information.

4 Concluding remarks

This work investigated the use commercially available scanning laser components for REP concentration, translation, and patterning. System features are similar to that of optical trapping systems; its cost could be further reduced by replacing or omitting more expensive components including the dual-turret inverted microscope, fluorescent components, and the low-noise CCD camera. However, these features were necessary for experimental observation of temperature, fluid velocimetry, and electrokinetic particle behavior. The electrokinetic behavior of the fluid dynamics and particle manipulation were discussed, which is governed primarily by heat transfer characteristics of the device. Device design to tune the heat transfer and temperature gradients will be a future focus.

Results presented herein were conducted at a constant laser power and AC field potential. Fluid velocity and particle concentration are functions of these variables [10]. In future work, we will vary these parameters to optimize particle translation and patterning, including the control of particle–particle spacing within the aggregation. The oscillatory nature of the electrothermal fluid dynamics observed in this work could be used to sort particles based on hydrodynamic drag, or enhance microfluidic mixing.

The authors would like to acknowledge ThorLabs, Inc. for assistance with the design and assembly of the system. V. Velasco acknowledges the support of the Southern Regional Education Board's Doctoral Scholarship. Dr. S. J. Williams acknowledges the support from start-up funds from the Mechanical Engineering and Bioengineering departments at the University of Louisville.

The authors have declared no conflict of interest.

5 References

[1] Xie, R., Liu, X.-Y., *J. Am. Chem. SOC* 2009, *131*, 4976–4982.

[2] Lumsdon, S. O., Kaler, E. W., Velev, O. D., *Langmuir* 2004, *20*, 2108–2116.

[3] Fiedler, S., Shirley, S. G., Schnelle, T., Fuhr, G., *Anal Chem.* 1998, *70*, 1909–1915.

[4] Ng, W. Y., Goh, S., Lam, Y. C., Yang, C., Rodriguez, I., *Lab Chip* 2009, *9*, 802–809.

[5] Gonzalez, A., Ramos, A., Morgan, H., Green, N. G., Castellanos, A., *J. Fluid Mech.* 2006, *564*, 415–433.

[6] Chiou, P. Y., Ohta, A. T., Wu, M. C., *Nature* 2005, *436*, 370–372.

[7] Ohta, A. T., Chiou, P., Han, T. H., Liao, J. C., Bhardwaj, U., McCabe, E. R. B., Yu, F., Sun, R., Wu, M. C., *J. Microelectromech. S.* 2007, *169*, 491–499.

[8] Valley, J. K., Jamshidi, A., Ohta, A. T., Hsu, H. Y., Wu, M. C., *J. Microelectromech. S.* 2008, *17*, 342–350.

[9] Williams, S. J., Kumar, A., Wereley, S. T., *Lab Chip* 2008, *8*, 1879–1882.

[10] Williams, S. J., Kumar, A., Green, N. G., Wereley, S. T., *J. Micromech. Microeng.* 2010, *20*, 015022.

[11] Kumar, A., Williams, S. J., Chuang, H. S., Green, N. G., Wereley, S. T., *Lab Chip* 2011, *11*, 2135–2148.

[12] Grier, D. G., *Nature* 2003, *424*, 810–816.

[13] Bechhoefer, J., Wilson, S., *Am. J. Phys.* 2002, *70*, 393–400.

[14] Kumar, A., Kwon, J.-S., Williams, S. J., Green, N. G., Yip, N. K., Wereley, S. T., *Langmuir* 2010, *26*, 5262–5272.

[15] Kumar, A., Williams, S. J., Wereley, S. T., *Microfluid. Nanofluid.* 2009, *6*, 637–646.

[16] Green, N. G., Ramos, A., Gonzalez, A., Castellanos, A., Morgan, H., *J. Electrostat.* 2001, *53*, 71–87.

[17] Ramos, A., Morgan, H., Green, N. G., Castellanos, A., *J. Phys. D Appl. Phys.* 1998, *31*, 2338–2353.

[18] Mizuno, A., Nishioka, M., Ohno, Y., Dascalescu, L. D., *IEEE T. Ind. Appl.*1995, *31*, 464–468.

[19] Nakano, M., Katsura, S., Touchard, G. G., Takashima, K., Mizuno, A., *IEEE T. Ind. Appl.* 2007, *43*, 232–237.

[20] Kumar, A., Cierpka, C., Williams, S. J., Kahler, C. J., Wereley, S. T., *Microfluid. Nanofluid.* 2010, *10*, 355–365.

[21] Castellanos, A., Ramos, A., Gonzalez, A., Green, N. G., Morgan, H., *J. Phys D Appl. Phys.* 2003, *36*, 2584–2597.

[22] Schwan, H. P., Schwarz, G., Maczuk, J., Pauly, H., *J. Phys. Chem.* 1962, *66*, 2626–2635.

[23] Schwarz, G., *J. Phys. Chem.* 1962, *66*, 2636–2642.

[24] Ross, D., Gaitan, M., Locascio, L. E., *Anal Chem.* 2001, *73*, 4117–4123.

[25] Williams, S. J., Chamarthy, P., Wereley, S. T., *J. Fluid. Eng.* 2010, *132*, 021103.

[26] Gui, L., Merzkirch, W., *Exp. Fluids* 1998, *24*, 66–69.

